Editors' Suggestion

Collective Excitations in Chiral Stoner Magnets

Zhiyu Dong, Olumakinde Ogunnaike, and Leonid Levitov
Department of Physics, Massachusetts Institute of Technology, Cambridge, Massachusetts 02139, USA

(Received 5 January 2023; revised 21 February 2023; accepted 7 April 2023; published 16 May 2023)

We argue that spin- and valley-polarized metallic phases recently observed in graphene bilayers and trilayers support chiral edge modes that allow spin waves to propagate ballistically along system boundaries without backscattering. The chiral edge behavior originates from the interplay between the momentum-space Berry curvature in Dirac bands and the geometric phase of a spin texture in position space. The edge modes are weakly confined to the edge, featuring dispersion that is robust and insensitive to the detailed profile of magnetization at the edge. This unique character of edge modes reduces their overlap with edge disorder and enhances the mode lifetime. The mode propagation direction reverses upon reversing valley polarization, an effect that provides a clear testable signature of geometric interactions in isospin-polarized Dirac bands.

DOI: 10.1103/PhysRevLett.130.206701

Stoner ferromagnetism is a correlated electron order ubiquitous in topological materials of current interest, including moiré graphene [1–6] and nontwisted graphene bilayers and trilayers [7–11]. Yet, the fundamental properties of this state, especially those governed by Berry curvature in k space, are presently poorly understood. Here we predict that this state hosts chiral spin excitations. These excitations are confined to system edges and domain boundaries between different valley-polarized regions, propagating along them in a manner resembling quantum Hall (QH) edge states, as illustrated in Fig. 1. The microscopic origin of this behavior is the geometric phase of carrier spins tracking magnetization along carrier trajectories. Carrier spin rotation by a position-dependent magnetization generates a Berry phase in direct space that serves as a spin-dependent magnetic vector potential that couples to the orbital dynamics of carriers [see Eqs. (4) and (5)] [12–15]. Chiral edge behavior arises due to coupling between this geometric magnetic field and the orbital magnetization due to Berry curvature in k space. The geometric character of this interaction ensures robust chiral edge physics even in "vanilla" spin-polarized Fermi seas, such as those seen in Refs. [7–11].

The band magnetism of carriers exhibiting orbital magnetization is a broad framework applicable to a diverse range of systems. This includes, in particular, the QH ferromagnets [16–19] and correlated excitonic phases in QH bilayers [20–24]. Orbital magnetization in these systems exists due to Landau levels rather than the k-space Berry curvature, and in QH bilayers, the layer index plays the role of spin in our analysis. Here we focus on chiral edges in spin-polarized metals and, afterward, comment on possible extensions to the QH systems.

In graphene multilayers [7–11], the predicted chiral edge behavior is sensitive to valley polarization. In a valley- and spin-polarized phase (identified as a quarter metal in Refs. [7–11]), the band orbital magnetization exhibits opposite signs in valleys K and K'. As a result, the chirality (i.e., the propagation direction) of edge modes flips upon reversing the valley imbalance. A very different behavior is expected in a valley-unpolarized but spin-polarized phase (half-metal in the nomenclature of Refs. [7–11]). In this case, the two valleys host Stoner metals with the band orbital magnetization of opposite signs. In this phase, the edges will host pairs of counterpropagating chiral edge modes, one for each valley. These two modes together

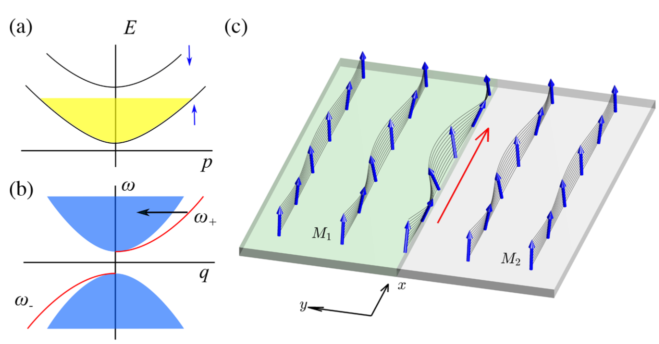

FIG. 1. (a) Schematic band structure of a fully spin-polarized Stoner phase in a valley-polarized graphene bilayer or trilayer band. Only the valley populated by carriers is shown. (b) The spin-wave edge mode dispersion obtained for a step in orbital magnetization $M_1 \neq M_2$ induced by a gate, Eq. [12]. The mode (red) is positioned outside the bulk magnon continuum (blue). The group velocity $v_g = d\omega/dq$ of a constant sign indicates the chiral character of the mode. The edge-to-bulk scattering (black arrow) is blocked by the energy and momentum conservation. (c) Schematic of the spatial dependence of the edge mode. The mode is confined to the step and propagates along it without backscattering.

respect the orbital time reversal symmetry, unbroken in the half-metal phase, i.e., the system is nonchiral.

The exceptional cleanness of graphene multilayers makes them an appealing system to probe this behavior. Spin lifetimes as long as 6 ns measured in large bilayer graphene (BLG) systems by a nonlocal Hanle effect at 20 K [25] are explained by residual magnetic disorder [26,27]. In contrast, recently, it was demonstrated that electrons isolated from edge disorder by gate confinement and trapped in gate-defined quantum dots acquire ultralong spin lifetimes, reaching values of 200 μs [28] and 50 ms [29] when measured in an applied magnetic field by pulsed-gate spectroscopy. Therefore, probing spin excitations in gate-defined electron puddles presents a distinct advantage. Yet, spin lifetimes measured in large BLG systems [25] also lie in a suitable range. Spin lifetimes can be further increased by applying nonquantizing magnetic fields that, apart from a constant offset, have little impact on the chiral spin-wave dispersion [see Eq. (18)].

In a metallic state, the chiral mode at the edge can, in principle, decay by scattering into the 2D spin-1 particle-hole continuum and spin waves. The former process is blocked by energy conservation since the spin-1 continuum is gapped at small momenta [see Supplemental Material [30] Fig. S1(a)]. The latter process, as shown by the black arrow in Fig. 1(b), is blocked by the energy and momentum conservation for a smooth edge, but can be viable for a rough edge. However, as discussed in the Supplemental Material [30], in the long-wavelength limit, the edge modes have vanishing overlaps with the edge disorder potential, a property that protects the modes from edge-to-bulk scattering.

The chiral edge behavior in a Stoner metal phase discussed here is distinct from that predicted for magnetic phases with a nontrivial magnon band topology [31–37]. In these systems, chiral edge excitations lie above the first magnon band and are therefore gapped. To the contrary, the chiral modes described here arise at the boundary of a uniformly spin-polarized Stoner Fermi sea—a metallic compressible state with a nontopological bulk magnon band. The edge excitations are gapless (in the absence of an externally applied magnetic field, see below) and have dispersion positioned beneath that of bulk spin waves (in our case, these are nothing but the gapless magnons of a Heisenberg ferromagnet). Accordingly, here chiral modes arise in the absence of microscopic spin-dependent interactions, such as Dzyaloshinskii-Moriya interaction or dipolar interaction (as in Refs. [31–35] and Refs. [36,37], respectively). Instead, they originate from an interplay between the exchange interaction and orbital magnetization in bands with Berry curvature and broken time reversal symmetry. Our spin waves act analogously to the chiral edge plasmons predicted for such bands [38], yet they transport spin rather than charge and arise from a very different mechanism.

Collective spin dynamics, both bulk and edge, are readily analyzed in the long-wavelength limit, at frequencies below the Stoner continuum [see Fig. S1(a) [30]],

$$\Delta = Un_s > \omega(q), \qquad (1)$$

where Δ is the Stoner gap, U is the exchange interaction, n_s is spin-polarized carrier density, and $\omega(q)$ is mode dispersion. We employ an effective action for spin variables obtained by integrating out fermion orbital degrees of freedom. In that, we assume the electron velocity is large compared to that of spin waves, $v_F \gg v_g = d\omega/dk$. As found below, the long-wavelength spin-wave dispersion is quadratic, $\omega(k) \sim k^2$, a behavior that confirms the separation of timescales for the orbital and spin degrees of freedom and justifies our analysis. The effective action for spin variables takes the form (see, e.g., [39,40])

$$A = \int dt d^2 r (i n_s S_0 \langle \eta(\boldsymbol{r},t)|\partial_t|\eta(\boldsymbol{r},t)\rangle - \mathcal{H}[\boldsymbol{n}]), \qquad (2)$$

where the first term is the Wess-Zumino-Witten action, hereafter referred to as A_{WZW}, representing the single-spin Berry phase accumulated through time evolution. The second term is the Hamiltonian of a spin-polarized state discussed below. The quantity $|\eta(\boldsymbol{r},t)\rangle$ represents a coherent spin state in $(2+1)$D space-time. Here $n_s = n_\uparrow - n_\downarrow$ is the density of spin-imbalanced carriers, and the factor $n_s S_0$ is the spin density, where $S_0 = \hbar/2$. In what follows, spin polarization is described by a unit vector,

$$\boldsymbol{n}(\boldsymbol{r},t) = \langle \eta(\boldsymbol{r},t)|\boldsymbol{\sigma}|\eta(\boldsymbol{r},t)\rangle.$$

The term $\mathcal{H}[\boldsymbol{n}]$ in Eq. (2) is the effective spin Hamiltonian. Symmetry arguments and microscopic analysis predict [41] the long-wavelength Hamiltonian

$$\mathcal{H}[\boldsymbol{n}] = n_s\left[\frac{J}{2}(\partial_\mu \boldsymbol{n})^2 - M(r)B(\boldsymbol{r},t) - \boldsymbol{h}_0\cdot\boldsymbol{n}\right]. \qquad (3)$$

Here J is spin stiffness, the second term is an interaction between the band orbital magnetization and the geometric magnetic field, and the last term is the Zeeman energy per carrier, with the g factor and Bohr magneton absorbed in the external magnetic field $\boldsymbol{h}_0$.

As indicated above, the interaction $-MB$ originates from a geometric Berry phase, arising due to electron spins tracking magnetization along electron trajectories. Spin rotation generates a Berry phase in position space defined by a spin-dependent magnetic vector potential [12]

$$a_\mu = \frac{\hbar c}{2e}(1-\cos\theta)\partial_\mu\phi, \qquad \mu = x, y. \qquad (4)$$

Here θ and ϕ are the polar and azimuthal angles measured with respect to the spin polarization axis in the ground state.

The sign of a_μ is chosen to describe the Berry phase accrued by the majority-spin carriers. For the minority-spin carriers, the vector potential is described by $-a_\mu$, giving a Berry phase of the opposite sign. The geometric magnetic field is simply the curl of a_μ. In terms of $\boldsymbol{n}$, it reads

$$B(\boldsymbol{r},t) = \nabla \times \boldsymbol{a} = \frac{\phi_0}{4\pi}\boldsymbol{n}\cdot(\partial_x \boldsymbol{n}\times\partial_y \boldsymbol{n}), \tag{5}$$

where $\phi_0 = hc/e$ is the flux quantum. This physics was first discussed in the early literature on high T_c superconductivity [42–45] and later in the literature on noncollinear magnetic systems [12–15]. Importantly, unlike static spin textures in the latter systems, our spin-wave dynamics generate a time-dependent vector potential, Eq. (4). This leads to a geometric electric field [14,46]

$$E_\mu = -\partial a_\mu / c\partial t - \nabla a_0 = \frac{\hbar}{2e}\boldsymbol{n}\cdot(\partial_t \boldsymbol{n}\times\partial_\mu \boldsymbol{n}), \tag{6}$$

which can enable electrical detection of the spin waves.

The quantity $M(r)$ in the second term in Eq. (3) describes the orbital magnetization per carrier in a spin-imbalanced band arising due to Berry curvature in k space. It is given by a sum of contributions of the filled states in the spin-valley-polarized Fermi sea. For a partially spin-polarized Fermi sea, the contributions to M from the majority- and minority-spin carriers are of opposite signs, giving $M = M_\uparrow - M_\downarrow$. The opposite signs originate from the opposite signs of a_μ for the spin-up and spin-down carriers discussed beneath Eq. (4). These opposite sign contributions cancel in a spin-unpolarized state, but lead to $M \neq 0$ in a fully or partially spin-polarized state. The position dependence $M(r)$ reflects spatially varying spin or valley imbalance arising, e.g., due to gating.

The geometric fields a_μ, B, and $\boldsymbol{E}_\mu$ are derived in the adiabatic regime when an electron spin tracks spin texture along the electron's trajectory. The adiabatic regime occurs when the spin texture is of sufficiently long wavelength, such that the Stoner spin gap $\Delta = Un_s$ is much greater than $\hbar v_F q$, where q is the characteristic spin-wave wave number and U is the exchange interaction [see Eq. (1)].

The Hamiltonian (3) features different phases depending on the M and J values [41]. If $M > 2J$ and h_0 is small enough, the uniformly polarized state is predicted to become unstable toward twisting, giving rise to a skyrmion texture with a nonzero chiral density B. Here, we consider excitations in a uniformly polarized state

$$\boldsymbol{n}(r,t) = \boldsymbol{n}_0 + \delta\boldsymbol{n}(r,t), \qquad \delta\boldsymbol{n}\perp\boldsymbol{n}_0, \tag{7}$$

with $\boldsymbol{n}_0 \| \boldsymbol{h}_0$, occurring for not too large M values.

The spin-wave dispersion can be obtained from the canonical equations of motion found from the saddle-point condition $\delta A/\delta\boldsymbol{n} = 0$, with A given in Eq. (2). Indeed, the variation of the Wess-Zumino-Witten term A_{WZW} [the first term in Eq. (2)] can be found by noting that this term equals $n_s S_0$ times the solid angle swept by $\boldsymbol{n}$. As a result, its variation can be expressed as

$$\delta A_{\mathrm{WZW}} = n_s S_0 \int dt d^2 r (\delta\boldsymbol{n}\times\partial_t \boldsymbol{n})\cdot\boldsymbol{n}. \tag{8}$$

The variation of the action in Eq. (2) gives $\delta A = (n_s S_0 \partial_t \boldsymbol{n}\times\boldsymbol{n} - \delta\mathcal{H}/\delta\boldsymbol{n})\cdot\delta\boldsymbol{n}$, giving equations of motion,

$$n_s S_0 \partial_t \boldsymbol{n}(r) = \boldsymbol{h}(r)\times\boldsymbol{n}(r), \qquad \boldsymbol{h} = -\frac{\partial\mathcal{H}}{\partial\boldsymbol{n}} + \partial_\mu \frac{\partial\mathcal{H}}{\partial\partial_\mu \boldsymbol{n}}. \tag{9}$$

Linearizing about a uniformly polarized state yields coupled linear equations for $\delta\boldsymbol{n}$ components, which are identical to those found for a nonchiral problem,

$$S_0 \partial_t \delta\boldsymbol{n}(r,t) = \boldsymbol{h}_0 \times \delta\boldsymbol{n}(r,t) + J\partial_\mu^2 \delta\boldsymbol{n}(r,t)\times\boldsymbol{n}_0. \tag{10}$$

Plane wave solutions to this equation yield a simple isotropic and nonchiral spin-wave dispersion

$$\omega_\pm(q) = \pm(h_0 + Jq^2)/S_0, \tag{11}$$

with values approaching $\pm h_0/S_0$ in the limit $q \to 0$, universally and independent of the exchange interaction, as required by the Larmor theorem.

For a spatially uniform M, the $-MB$ term is a topological invariant. Therefore, a local twist of spin does not change the $\mathcal{H}$ value. As a result, this interaction neither affects the energy nor impacts the spin waves. A spatially varying M, to the contrary, has a profound effect on spin waves. In particular, system boundaries and interfaces between regions in which M takes different values support chiral spin-wave modes reminiscent of the QH edge states. To illustrate this behavior, we consider a step

$$M(y) = \begin{cases} M_1, & y > 0, \\ M_2, & y < 0. \end{cases} \tag{12}$$

In this case, after linearization (7), we find

$$\boldsymbol{h} = n_s[J\partial_\mu^2 \delta\boldsymbol{n} - \partial_y M(y)(\boldsymbol{n}_0 \times \partial_x \delta\boldsymbol{n}) + \boldsymbol{h}_0]. \tag{13}$$

Other terms vanish at first order in $\delta\boldsymbol{n}$. As a result, the linearized equations of motion become

$$S_0 \partial_t \delta\boldsymbol{n} = \boldsymbol{h}_0 \times \delta\boldsymbol{n} + J\partial_\mu^2 \delta\boldsymbol{n}\times\boldsymbol{n}_0 + m\delta(y)(\boldsymbol{n}_0 \times \partial_x \delta\boldsymbol{n})\times\boldsymbol{n}_0,$$

where $m = M_2 - M_1$ is the difference between M on two sides of the edge. These equations are solved by writing $\delta\boldsymbol{n}(x,y)$ as a superposition of complex-valued helical components,

$$\delta\boldsymbol{n}(r,t)=\begin{pmatrix}\delta n_x(r,t)\\ \delta n_y(r,t)\end{pmatrix}=\sum_q e^{iqx}\left[e^{-i\omega_+t}\psi_{q,+}(y)\begin{pmatrix}1\\ i\end{pmatrix}+e^{-i\omega_-t}\psi_{q,-}(y)\begin{pmatrix}1\\ -i\end{pmatrix}\right] \quad (14)$$

where we carried out the Fourier transform in time and the translation-invariant x direction. Plugging this ansatz into the equations of motion for $\delta\boldsymbol{n}(r,t)$, we obtain two decoupled 1D problems for a quantum particle in a delta-function potential, separately for each helicity:

$$S_0\omega_\pm\psi(y)=\pm[h_0+J(q^2-\partial_y^2)]\psi(y)-mq\delta(y)\psi(y), \quad (15)$$

where $\psi(y)$ is a shorthand for $\psi_{q,\pm}(y)$. These equations support bound states that are edge spin waves for the helical polarization of a plus (minus) sign for mq of a positive (negative) sign, respectively.

Indeed, the bound state is described by an exponential solution for both helicities,

$$\psi_{q,\pm}(y)=u_q e^{-\lambda_q|y|}, \qquad \lambda_q>0, \quad (16)$$

where the condition $\lambda_q>0$ is required for the mode to be normalizable. The value of λ_q and the dispersion are determined by the condition

$$0=\pm 2J\lambda_q\delta(y)-mq\delta(y), \quad (17)$$

which gives $\lambda_q=\pm(mq/2J)$. Therefore, the right-helicity mode ψ_+ exists only for $mq>0$, whereas the left-helicity mode ψ_- exists only for $mq<0$,

$$\omega_\pm(q)=\pm\frac{1}{S_0}\left[h_0+\left(J-\frac{m^2}{4J}\right)q^2\right]. \quad (18)$$

The resulting dispersion is illustrated in Fig. 1(b) for $m>0$. The group velocity $v_g=d\omega/dq$ is of the same sign for both helicities, as expected for a chiral edge mode. At $q=0$, the frequency value agrees with the Zeeman frequency for a single spin, as required by Larmor's theorem. At this point λ_q vanishes, which signals that the mode ceases to be confined to the edge and transforms into a uniformly precessing state.

Notably, the discrete chiral mode (18) appears in a robust manner regardless of magnetization values in the two half-planes and the step size $m=M_1-M_2$. At M_1 approaching M_2, the chiral mode, while remaining discrete, approaches the bulk magnon continuum and merges with it at $M_1=M_2$. Another interesting aspect of the dispersion in Eq. (18) is that the group velocity reverses when m exceeds $2J$, upon which the mode propagation direction is reversed, with the left-moving excitations becoming right-moving and vice versa. In this regime, the frequencies $\omega_\pm(q)$ reverse their signs when the wave number reaches a certain critical value, $q=q_*=\sqrt{4Jh_0/(4J^2-m^2)}$. Frequency sign reversal signals an instability toward a spatial modulation at the edge with spatial periodicity $2\pi/q_*$. Notably, this instability can occur before skyrmions are nucleated in the bulk. This happens, in particular, when M_1 and M_2 are of opposite signs. In this case, the condition for skyrmion nucleation in the bulk, $2J<|M_{1,2}|$, is more stringent than that for the instability at the edge, $2J<|M_1-M_2|$.

Next, we consider polarization of chiral modes. As we found above, the modes of both helicities ψ_+ and ψ_- propagate in the same direction. This gives rise to an interesting space-time picture that combines propagation with velocity v_g and precession about $\boldsymbol{h}_0$. Indeed, a narrow wave packet u_q centered at $q\approx q_0$ evolves as

$$\delta\boldsymbol{n}(r,t)=\sum_{q>0}\phi_q^+(r,t)\begin{pmatrix}1\\ i\end{pmatrix}+\sum_{q<0}\phi_q^-(r,t)\begin{pmatrix}1\\ -i\end{pmatrix}\sim e^{-\lambda_{q_0}|y|}u(x-v_gt)\begin{pmatrix}\cos[\omega_0t-q_0x+\theta_0]\\ \sin[\omega_0t-q_0x+\theta_0]\end{pmatrix}. \quad (19)$$

Here, $\phi_q^\pm(r,t)=e^{-i\omega_\pm(q)t+iqx-\lambda_q|y|}u_q$. The quantity $u(x)$ is the Fourier transform of u_q, $\omega_0=\omega_+(q_0)$, v_g is the group velocity $d\omega/dq$ at $q=q_0$, θ_0 is a free parameter. This describes spin precession and 1D propagation as illustrated in Fig. 1(c).

Last, we discuss the relation between the analysis above and the collective spin excitations in QH ferromagnets. The seminal prediction of skyrmions in QH ferromagnets by Sondhi *et al.* [47] relies on the notion of an excess charge induced on a chiral spin texture, $\delta\rho(r)=\frac{1}{c}\sigma_{xy}B(r)$, a value that follows from the topological pumping argument [48,49], with σ_{xy} the Hall conductivity of a filled Landau level and B the quantity in Eq. (5). This gives a contribution to the energy

$$\delta E=\int d^2rV_g\delta\rho(r), \quad (20)$$

where V_g is the gate voltage. Since $B(r)=(\phi_0/4\pi)\boldsymbol{n}\cdot\partial_x\boldsymbol{n}\times\partial_y\boldsymbol{n}$, the quantity in Eq. (20) is identical in form to our $-MB$ interaction [the second term in Eq. (3)]. Furthermore, it is straightforward to link the prefactor with the orbital magnetization of a fully filled Landau level,

$$M=\frac{1}{c}V_g\sigma_{xy}. \quad (21)$$

This relation follows from the thermodynamic relation $dM/d\mu=dn/dB_{\text{ext}}$ and the Streda formula $dn/dB_{\text{ext}}=(\sigma_{xy}/ce)$. Having reproduced the $-MB$ interaction, we are led to conclude that the chiral spin waves derived above must also occur in QH ferromagnets. While a detailed analysis should be deferred to future work, we expect that these modes differ in two distinct ways from various chiral charge and spin edge modes that have been widely investigated in QH systems [50–58]. First, their dispersion at small k will be quadratic rather than linear. Second, rather than being tightly confined to the edge on a magnetic length scale, these modes will feature a wider profile extending far into the bulk. The weak confinement may suppress scattering by edge disorder and boost the lifetimes for these modes.

Last, we envision that extending the pulsed-gate spectroscopy of Refs. [28,29] to probe the gate-confined electron puddles can allow one to launch the chiral spin waves and detect them in a manner analogous to the time-domain detection of QH edge magnetoplasmons [59–62]. Further, electron-spin resonance (ESR) measurements on such puddles by the technique recently used to probe ESR in graphene [63] can provide direct information of the chiral mode dispersion. Indeed, for a puddle of circumference L, the mode dispersion in Eq. (18) will translate into sidebands of the ESR resonance with frequencies

$$\omega_n = \omega(q_n), \qquad q_n = 2\pi n/L, \tag{22}$$

with integer n. Here $n = 0$ is the fundamental ESR frequency and $n = 1, 2, 3\ldots$ describes a family of chiral mode excitations. The $\omega = \omega_n$ resonances will occur over a continuous background due to the 2D spin-wave continuum, Eq. (11). As an example, we consider a disk of circumference $L = 10$ μm for which the minimal wave number is $q_1 = 2\pi/L$. Estimating the stiffness as the $e - e$ interaction at the Fermi wavelength scale, $J \sim e^2/(\kappa\lambda_F)$, and plugging realistic parameter values, we find the sideband frequency detuning of $\omega_1 - \omega_0 \approx 50$ MHz. This value is greater than $1/T_1$ found in Refs. [28,29] and lies in a convenient range for microwave measurements. We also note that, as discussed above, spin dynamics in our system is accompanied by a geometric electric field given in Eq. (6). The oscillating electric polarization induced by this field can be used for a direct electrical detection of the chiral spin-wave dynamics.

Summing up, the chiral edge excitations are a unique manifestation of geometric interactions in a metallic spin-polarized Fermi sea with a Berry band curvature. Despite occurring in a nontopological setting, they are protected from backscattering by their chiral character. Correlated-electron phases that host chiral edge modes allowing excitations to propagate along system boundaries in a one-way manner are of keen interest for fundamental physics and are expected to harbor interesting applications. We describe the requirements for such modes to exist and argue that the chiral behavior and associated exotic physics are generic and readily accessible in state-of-the-art systems.

This work originated from fruitful discussions with Eli Zeldov. We thank Herbert Fertig, Steven Girvin, Bertrand Halperin, Efrat Shimshoni, Shivaji Sondhi and Kun Yang for useful comments on the preliminary version of this paper. This research was supported by the Science and Technology Center for Integrated Quantum Materials, National Science Foundation Grant No. DMR1231319.

[1] E. Y. Andrei and A. H. MacDonald, Graphene bilayers with a twist, Nat. Mater. **19**, 1265 (2020).

[2] Y. Cao, V. Fatemi, A. Demir, S. Fang, S. L. Tomarken, J. Y. Luo, J. D. Sanchez-Yamagishi, K. Watanabe, T. Taniguchi, E. Kaxiras *et al.*, Correlated insulator behaviour at half-filling in magic-angle graphene superlattices, Nature (London) **556**, 80 (2018).

[3] Y. Cao, V. Fatemi, S. Fang, K. Watanabe, T. Taniguchi, E. Kaxiras, and P. Jarillo-Herrero, Unconventional superconductivity in magic-angle graphene superlattices, Nature (London) **556**, 43 (2018).

[4] U. Zondiner, A. Rozen, D. Rodan-Legrain, Y. Cao, R. Queiroz, T. Taniguchi, K. Watanabe, Y. Oreg, F. von Oppen, A. Stern, E. Berg, P. Jarillo-Herrero, and S. Ilani, Cascade of phase transitions and dirac revivals in magic-angle graphene, Nature (London) **582**, 203 (2020).

[5] D. Wong, K. P. Nuckolls, M. Oh, B. Lian, Y. Xie, S. Jeon, K. Watanabe, T. Taniguchi, B. A. Bernevig, and A. Yazdani, Cascade of electronic transitions in magic-angle twisted bilayer graphene, Nature (London) **582**, 198 (2020).

[6] Y. Saito, F. Yang, J. Ge, X. Liu, T. Taniguchi, K. Watanabe, J. Li, E. Berg, and A. F. Young, Isospin Pomeranchuk effect in twisted bilayer graphene, Nature (London) **592**, 220 (2021).

[7] H. Zhou, L. Holleis, Y. Saito, L. Cohen, W. Huynh, C. L. Patterson, F. Yang, T. Taniguchi, K. Watanabe, and A. F. Young, Isospin magnetism and spin-polarized superconductivity in Bernal bilayer graphene, Science **375**, 774 (2022).

[8] A. M. Seiler, F. R. Geisenhof, F. Winterer, K. Watanabe, T. Taniguchi, T. Xu, F. Zhang, and R. T. Weitz, Quantum cascade of new correlated phases in trigonally warped bilayer graphene, Nature (London) **608**, 298 (2022).

[9] S. C. de la Barrera, S. Aronson, Z. Zheng, K. Watanabe, T. Taniguchi, Q. Ma, P. Jarillo-Herrero, and R. Ashoori, Cascade of isospin phase transitions in Bernal bilayer graphene at zero magnetic field, Nat. Phys. **18**, 771 (2022).

[10] H. Zhou, T. Xie, A. Ghazaryan, T. Holder, J. R. Ehrets, E. M. Spanton, T. Taniguchi, K. Watanabe, E. Berg, M. Serbyn, and A. F. Young, Half-and quarter-metals in rhombohedral trilayer graphene, Nature (London) **598**, 429 (2021).

[11] H. Zhou, T. Xie, T. Taniguchi, K. Watanabe, and A. F. Young, Superconductivity in rhombohedral trilayer graphene, Nature (London) **598**, 434 (2021).

[12] K. Ohgushi, S. Murakami, and N. Nagaosa, Spin anisotropy and quantum Hall effect in the kagomé lattice: Chiral spin state based on a ferromagnet, Phys. Rev. B **62**, R6065 (2000).

[13] T. Fujita, M. Jalil, S. Tan, and S. Murakami, Gauge fields in spintronics, J. Appl. Phys. **110**, 17 (2011).

[14] N. Nagaosa and Y. Tokura, Emergent electromagnetism in solids, Phys. Scr. **2012**, 014020 (2012).

[15] K. Hamamoto, M. Ezawa, and N. Nagaosa, Quantized topological Hall effect in skyrmion crystal, Phys. Rev. B **92**, 115417 (2015).

[16] S. M. Girvin, Spin and isospin: Exotic order in quantum Hall ferromagnets, Phys. Today **53**, No. 6, 39 (2000).

[17] K. Nomura and A. H. MacDonald, Quantum Hall Ferromagnetism in Graphene, Phys. Rev. Lett. **96**, 256602 (2006).

[18] J. Alicea and M. P. A. Fisher, Graphene integer quantum Hall effect in the ferromagnetic and paramagnetic regimes, Phys. Rev. B **74**, 075422 (2006).

[19] K. Yang, S. Das Sarma, and A. H. MacDonald, Collective modes and skyrmion excitations in graphene SU(4) quantum Hall ferromagnets, Phys. Rev. B **74**, 075423 (2006).

[20] I. B. Spielman, J. P. Eisenstein, L. N. Pfeiffer, and K. W. West, Resonantly Enhanced Tunneling in a Double Layer Quantum Hall Ferromagnet, Phys. Rev. Lett. **84**, 5808 (2000).

[21] J. Eisenstein, Exciton condensation in bilayer quantum Hall systems, Annu. Rev. Condens. Matter Phys. **5**, 159 (2014).

[22] J. Eisenstein and A. MacDonald, Bose–Einstein condensation of excitons in bilayer electron systems, Nature (London) **432**, 691 (2004).

[23] J. Li, T. Taniguchi, K. Watanabe, J. Hone, and C. Dean, Excitonic superfluid phase in double bilayer graphene, Nat. Phys. **13**, 751 (2017).

[24] A. D. K. Finck, J. P. Eisenstein, L. N. Pfeiffer, and K. W. West, Quantum Hall Exciton Condensation at Full Spin Polarization, Phys. Rev. Lett. **104**, 016801 (2010).

[25] W. Han, K. McCreary, K. Pi, W. Wang, Y. Li, H. Wen, J. Chen, and R. Kawakami, Spin transport and relaxation in graphene, J. Magn. Magn. Mater. **324**, 369 (2012).

[26] D. Kochan, M. Gmitra, and J. Fabian, Spin Relaxation Mechanism in Graphene: Resonant Scattering by Magnetic Impurities, Phys. Rev. Lett. **112**, 116602 (2014).

[27] D. Kochan, S. Irmer, M. Gmitra, and J. Fabian, Resonant Scattering by Magnetic Impurities as a Model for Spin Relaxation in Bilayer Graphene, Phys. Rev. Lett. **115**, 196601 (2015).

[28] L. Banszerus, K. Hecker, S. Möller, E. Icking, K. Watanabe, T. Taniguchi, C. Volk, and C. Stampfer, Spin relaxation in a single-electron graphene quantum dot, Nat. Commun. **13**, 3637 (2022).

[29] L. M. Gächter, R. Garreis, J. D. Gerber, M. J. Ruckriegel, C. Tong, B. Kratochwil, F. K. de Vries, A. Kurzmann, K. Watanabe, T. Taniguchi, T. Ihn, K. Ensslin, and W. W. Huang, Single-shot spin readout in graphene quantum dots, PRX Quantum **3**, 020343 (2022).

[30] See Supplemental Material at http://link.aps.org/supplemental/10.1103/PhysRevLett.130.206701, where the decay of the edge mode due to Landau damping and due to edge-to-bulk scattering by the edge roughness is analyzed.

[31] A. Mook, J. Henk, and I. Mertig, Edge states in topological magnon insulators, Phys. Rev. B **90**, 024412 (2014).

[32] K. Mæland and A. Sudbø, Quantum topological phase transitions in skyrmion crystals, Phys. Rev. Res. **4**, L032025 (2022).

[33] S. A. Díaz, J. Klinovaja, and D. Loss, Topological Magnons and Edge States in Antiferromagnetic Skyrmion Crystals, Phys. Rev. Lett. **122**, 187203 (2019).

[34] F. Garcia-Sanchez, P. Borys, A. Vansteenkiste, J.-V. Kim, and R. L. Stamps, Nonreciprocal spin-wave channeling along textures driven by the Dzyaloshinskii-Moriya interaction, Phys. Rev. B **89**, 224408 (2014).

[35] P. A. McClarty, Topological magnons: A review, Annu. Rev. Condens. Matter Phys. **13**, 171 (2022).

[36] R. Shindou, R. Matsumoto, S. Murakami, and J.-i. Ohe, Topological chiral magnonic edge mode in a magnonic crystal, Phys. Rev. B **87**, 174427 (2013).

[37] R. Shindou, J.-i. Ohe, R. Matsumoto, S. Murakami, and E. Saitoh, Chiral spin-wave edge modes in dipolar magnetic thin films, Phys. Rev. B **87**, 174402 (2013).

[38] J. C. Song and M. S. Rudner, Chiral plasmons without magnetic field, Proc. Natl. Acad. Sci. U.S.A. **113**, 4658 (2016).

[39] N. Nagaosa, *Quantum Field Theory in Condensed Matter Physics* (Springer Berlin Heidelberg, 2013).

[40] E. Fradkin, *Field Theories of Condensed Matter Physics* (Cambridge University Press, 2013).

[41] Z. Dong and L. Levitov, Chiral Stoner magnetism in dirac bands, arXiv:2208.02051.

[42] G. Baskaran and P. W. Anderson, Gauge theory of high-temperature superconductors and strongly correlated Fermi systems, Phys. Rev. B **37**, 580 (1988).

[43] P. B. Wiegmann, Superconductivity in Strongly Correlated Electronic Systems and Confinement Versus Deconfinement Phenomenon, Phys. Rev. Lett. **60**, 821 (1988).

[44] H. J. Schulz, Effective Action for Strongly Correlated Fermions from Functional Integrals, Phys. Rev. Lett. **65**, 2462 (1990).

[45] L. B. Ioffe, V. Kalmeyer, and P. B. Wiegmann, Hall coefficient of the doped Mott insulator: A signature of parity violation, Phys. Rev. B **43**, 1219 (1991).

[46] C. Back, V. Cros, H. Ebert, K. Everschor-Sitte, A. Fert, M. Garst, T. Ma, S. Mankovsky, T. Monchesky, M. Mostovoy *et al.*, The 2020 skyrmionics roadmap, J. Phys. D **53**, 363001 (2020).

[47] S. L. Sondhi, A. Karlhede, S. A. Kivelson, and E. H. Rezayi, Skyrmions and the crossover from the integer to fractional quantum Hall effect at small Zeeman energies, Phys. Rev. B **47**, 16419 (1993).

[48] D. J. Thouless, Quantization of particle transport, Phys. Rev. B **27**, 6083 (1983).

[49] Q. Niu and D. Thouless, Quantised adiabatic charge transport in the presence of substrate disorder and many-body interaction, J. Phys. A **17**, 2453 (1984).

[50] N. Q. Balaban, U. Meirav, H. Shtrikman, and V. Umansky, Observation of the logarithmic dispersion of high-frequency edge excitations, Phys. Rev. B **55**, R13397 (1997).

[51] V. Mazo, H. A. Fertig, and E. Shimshoni, Collective edge modes of a quantum Hall ferromagnet in graphene, Phys. Rev. B **86**, 125404 (2012).

[52] P. Tikhonov, E. Shimshoni, H. A. Fertig, and G. Murthy, Emergence of helical edge conduction in graphene at the $\nu = 0$ quantum Hall state, Phys. Rev. B **93**, 115137 (2016).

[53] S. Iordanski and A. Kasbuba, Excitations in a quantum Hall ferromagnet with strong coulomb interaction, J. Exp. Theor. Phys. Lett. **75**, 348 (2002).

[54] A. Karlhede, K. Lejnell, and S. L. Sondhi, Dynamics of the compact, ferromagnetic $\nu = 1$ edge, Phys. Rev. B **60**, 15948 (1999).

[55] Y. Zhang and K. Yang, Edge spin excitations and reconstructions of integer quantum Hall liquids, Phys. Rev. B **87**, 125140 (2013).

[56] M. Kharitonov, S. Juergens, and B. Trauzettel, Interplay of topology and interactions in quantum Hall topological insulators: U(1) symmetry, tunable Luttinger liquid, and interaction-induced phase transitions, Phys. Rev. B **94**, 035146 (2016).

[57] A. Saha, S. J. De, S. Rao, Y. Gefen, and G. Murthy, Emergence of spin-active channels at a quantum Hall interface, Phys. Rev. B **103**, L081401 (2021).

[58] U. Khanna, M. Goldstein, Y. Gefen, Emergence of Neutral Modes in Laughlin-like Fractional Quantum Hall Phases, Phys. Rev. Lett. **129**, 146801 (2022).

[59] R. C. Ashoori, H. L. Stormer, L. N. Pfeiffer, K. W. Baldwin, and K. West, Edge magnetoplasmons in the time domain, Phys. Rev. B **45**, 3894 (1992).

[60] N. B. Zhitenev, R. J. Haug, K. v. Klitzing, and K. Eberl, Time-Resolved Measurements of Transport in Edge Channels, Phys. Rev. Lett. **71**, 2292 (1993).

[61] G. Ernst, R. J. Haug, J. Kuhl, K. von Klitzing, and K. Eberl, Acoustic Edge Modes of the Degenerate Two-Dimensional Electron Gas Studied by Time-Resolved Magnetotransport Measurements, Phys. Rev. Lett. **77**, 4245 (1996).

[62] N. Kumada, H. Kamata, and T. Fujisawa, Edge magnetoplasmon transport in gated and ungated quantum Hall systems, Phys. Rev. B **84**, 045314 (2011).

[63] J. Sichau, M. Prada, T. Anlauf, T. J. Lyon, B. Bosnjak, L. Tiemann, and R. H. Blick, Resonance Microwave Measurements of an Intrinsic Spin-Orbit Coupling Gap in Graphene: A Possible Indication of a Topological State, Phys. Rev. Lett. **122**, 046403 (2019).